CONFERENCE PRE-PRINT

UTILIZING A VISIBLE CAMERA IN THE FIRST OPERATION PHASE(S) OF A FUSION DEVICE

T. SZEPESI
HUN-REN Centre for Energy Research, Atomic Energy Research Institute
Budapest, Hungary
Email: szepesi.tamas@ek.hun-ren.hu

A. BUZÁS*, G. CSEH, G. KOCSIS, D.I. RÉFY
HUN-REN Centre for Energy Research, Atomic Energy Research Institute
*Institute of Nuclear Techniques, Budapest University of Technology and Economics
Budapest, Hungary

C. BIEDERMANN, M. JAKUBOWSKI, M. OTTE, V. PERSEO, W7-X TEAM
Max-Planck-Institut für Plasmaphysik
Greifswald, Germany

T. NAKANO, M. YOSHIDA, JT-60SA INTEGRATED PROJECT TEAM
National Institutes for Quantum Science and Technology
Naka, Japan

W. BIN, G. DE TOMMASI, D. RICCI, C. SOZZI
ISTP-CNR
Milano, Italy

F. FIORENZA, D. FRATTOLILLO, M. MATTEI, A. PIRONTI
Consorzio CREATE/DIETI Università di Napoli Federico II
Napoli, Italy

M. IAFRATI
Fusion Technology Division, ENEA
Frascati, Italy

Abstract

A visible video diagnostic system, based on the Event Detection Intelligent Camera, was installed at superconducting fusion experiments JT-60SA and Wendelstein 7-X. Both camera systems were operational from day 1, witnessing the first plasma attempts and contributing to the success of machine commissioning. In the early days of operation, when advanced diagnostic systems were not available, the visible video diagnostic provided essential feedback on the machine status for the operators. The achievement of plasma breakdown and burn-though, as well as the obtained plasma size could clearly be followed. More advanced analyses have proven the presence of runaway electrons during plasma ramp-down phases in JT-60SA discharges, utilizing the camera's sensor as a hard X-ray detector. At Wendelstein 7-X, a simple machine learning technique was applied to determine the onset and duration of divertor detachment.

1. INTRODUCTION

The past decade has witnessed the launch of two highly advanced fusion experiments. JT-60SA, the world's largest superconducting tokamak, entered integrated commissioning and first plasma operation (IC&OP1), achieving first plasma in October 2023 [1], while Wendelstein 7-X (W7-X), the world's largest superconducting stellarator, accomplished its first plasma in 2015 [2]. Both devices, although being the flagships of their kind, have carried out their first campaign with clearly limited diagnostic sets – at least compared to the (future) diagnostics palette (which would be) available many years after their start. JT-60SA completed IC&OP1 relying on data from a CO2 laser interferometer, a soft X-ray diagnostic system, and visible TV cameras, but lacked stray detectors for electron cyclotron (EC) heating waves – see complete list in [3]. Similarly, W7-X was also started with a basic set, although the list of 20 diagnostic systems is longer here, including stray radiation detectors [4].

Generally, fusion experiments in their early stage of life are equipped with a limited set of diagnostic systems – this state, on the other hand, is very similar to what is expected for future fusion reactors, although due to very different reasons. Experiments are started up as soon as possible, with diagnostics essential for safe operations, so that sufficient experience is earned to stably run the machine when advanced diagnostics systems are installed to gain new knowledge in physics. Different is for future fusion reactors, where cost efficiency and the industrial nature of the plant are the main driving forces for limiting the number and complexity of diagnostics. Nevertheless, the conditions in which the operators need to run these machines are very similar, and thus the start-up phases of new fusion experiments are valuable sources of experience for future reactors.

The paper directs the attention to one of the most basic diagnostic systems that the vast majority of fusion devices have: the visible video diagnostics. Both superconducting experiments featured an overview visible camera system based on the Event Detection Intelligent Camera (EDICAM) [5], operational from day 1: a single-camera system at JT-60SA [6], and a 10-channel camera system at W7-X [7]. The major aim of the paper is to show that the visible video is an indispensable diagnostic system for every magnetic fusion device; beyond the trivial operational and scientific benefits, camera images and recordings are especially significant from the human-factor point of view. Plasma operators, chief scientists and technicians are all people, and the human brain is trained to work with images. Hence, scientists will always have the urge, no matter how detailed data they get from other sources, to “see” what is happening inside an experiment; this helps them to understand the observed phenomena. The more pragmatic reason behind using visible video diagnostics is that the edge plasma radiation, as well as light emissions of plasma-wall interaction fall mostly in the visible range, which can be used for both plasma control and scientific purposes.

The paper is structured as follows: Section 2 presents, through camera snapshots of various machine states, the operational experience collected during the first plasma attempts at JT-60SA and W7-X; Section 3 and 4 shows the potential of video diagnostics via detailed image data analysis, detecting runaway electrons in JT-60SA and divertor detachment in W7-X.

2. MACHINE START-UP

Starting a fusion device for the first time is always an iterative process as the operators naturally have no experience with the specific machine, and need to adapt to various circumstances that cannot be known precisely in advance, e.g. actual wall conditions or impurity sources. First plasma attempts usually fail or result in very short discharges, while operators need to optimize the electromagnetic configuration and the use of external heating. The power of the heating waves is often poorly absorbed, and the wave bounces within the plasma vessel, creating small-volume plasmas in several localized regions. In such cases, visible camera images can provide valuable support for the operators to understand how exactly the plasma discharge evolved, which can confirm, refine or even contradict other – usually line-integrated or point-like – data sources.

FIG. 1. shows two examples of failed plasma attempts, one from JT-60SA (a) and one from W7-X (b). In the case of JT-60SA, two EC heating waves were used with 82 GHz and 110 GHz frequency. The images of the EDICAM provided a powerful tool study the heating absorption. It can be seen on image (a) that visible light is emitted in two distinct cylindrical patterns around the central column, which reveals the following:

— The two heating waves produce two, spatially localized, distinct plasmas having a thin cylindrical shape. Thus, no bulk plasma formation took place, the majority of the gas inventory was not ionized; in other words, **no burn-through was achieved**.
— The observed plasma shapes show cylindrical symmetry, which implies that only the vacuum magnetic field is present. Thus, no or only **negligible plasma current was induced**.
— The 110 GHz resonance layer (denoted by a dashed red line) features two brighter regions, which also extend toroidally. These regions coincide with the first crossing of the EC beam path with the resonance layer, and with the second and third crossing of the beam due to the first and second reflection on the wall. The beam path, tracked in 3D for two reflections and three crossings of the resonance layer, is projected onto the image in yellow. There is no brighter region seen at the third pass location, which implies that **most of the heating beam power is absorbed at the first and the second pass**.

A very similar evaluation can be carried out for the stellarator case, see FIG. 1. (b). The main difference is that even without plasma, the magnetic field is fully 3D in this case, hence the localized plasma created by the EC heating wave clearly follows a helical magnetic field line. This, however, is not that straightforward by looking

at the irregular, star-like emission, but if a magnetic field line (carefully selected to fit to the ECRH beam path), tracked for three toroidal turns, is projected onto the image, the observed pattern suddenly makes sense. Note that the camera view's perspective is such that the field line loops on itself or seems to be "bouncing" in the 2D projection (green line on the image). These differences between the tokamak and stellarator images originate clearly from the design of these devices, nevertheless the two cases show exactly the same machine status: a start-up attempt where the gas reservoir is not fully ionized, no bulk plasma was formed (also no plasma current in the tokamak case), only localized and thin plasma-filled regions were created, which are isolated from and filling only a small fraction of the vacuum vessel. In short: no burn-through was achieved.

Such images can help plasma operators to get a better understanding of the machine status, hance modify electromagnetic configuration, and the heating and fuelling scheme of the device to achieve successful discharges.

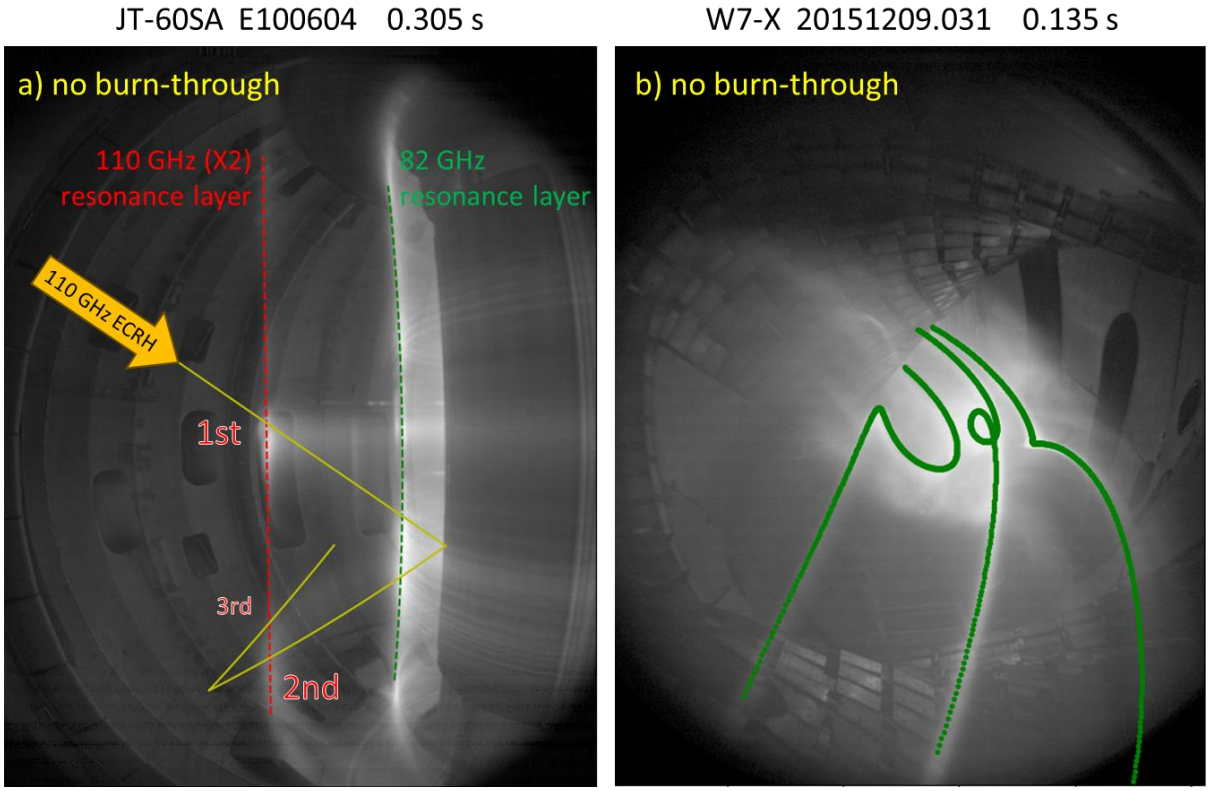

FIG. 1. First plasma attempts at JT-60SA (a) and Wendelstein 7-X (b). No burn-through was achieved, the heating waves create only thin, localized plasma regions, following the vacuum magnetic field lines.

Another common situation during the first operational campaign occurs when burn-through is achieved and stable tokamak or stellarator plasmas are formed, but no contact with plasma-facing components is detected by temperature sensors or Langmuir probes. In such cases, the plasma size remains unknown, and operators cannot determine whether their modifications have a beneficial influence or an adverse one. Visible camera images are especially useful in these cases because they allow for the observation of plasma size: in the plasma edge region electron temperature is low enough for visible light emission, while density is still high, resulting in strong line radiation dominated by the main plasma species (in most cases H-alpha or D-alpha). This translates to the appearance of a "radiation belt", a thin and bright region surrounding the hot (hence transparent) plasma, on visible camera images. Thus, *the radiation belt is a good proxy for the confined plasma's size*.

In tokamaks and other toroidally symmetric fusion devices, the shape of the radiation belt is very similar to that of magnetic flux surfaces; the plasma size can be easily inferred, even by comparison to in-vessel structures with known dimensions. A good example is the first tokamak plasma achieved in JT-60SA, shown in FIG. 2. (a). The radiation belt is seen in the middle of the image, within the red circle marking; its inboard side is bright and distinct, while the outboard side fades to the background of in-vessel components. Inferring the plasma size, the radiation belt can be compared to the large port opening P5, which has a height of 1.8 m. Since the port is further away, we can estimate the height of the plasma to be ca. 1.5 m. A more careful analysis, relying on flux surface

reconstruction using the CREATE filamentary model, reveals a plasma height of 1.4 m [8], which agrees fairly well with our rough estimate. One can clearly see the large gap between the belt and the heat shield of the central column; this, and the fact that no plasma-wall interaction is observed on any of the outer limiters in the view, shows that the plasma is obviously significantly smaller than the available space in the vacuum vessel.

The situation is again similar, but more complex for W7-X. FIG. 2. (b) displays a similar (but significantly brighter), oval radiation belt. However, this shape does not resemble the flux surfaces of the stellarator: the tangential camera view integrates all light emission along its lines-of-sight from various toroidal locations where the same flux surface has different shapes, ranging from triangular to bean-shaped. The integrated emission pattern yields an oval shape with wing-like protrusions. Because of this complex geometry, we should not compare the plasma size to in-vessel structures; the only solid point we can say is that the gap between the radiation belt and the inner heat shield is large, implying a plasma size again significantly smaller than the available space. On the other hand, a more careful analysis, comparing synthetic images to measured ones [9], can be used to determine the plasma size with reasonable precision even in this complex case.

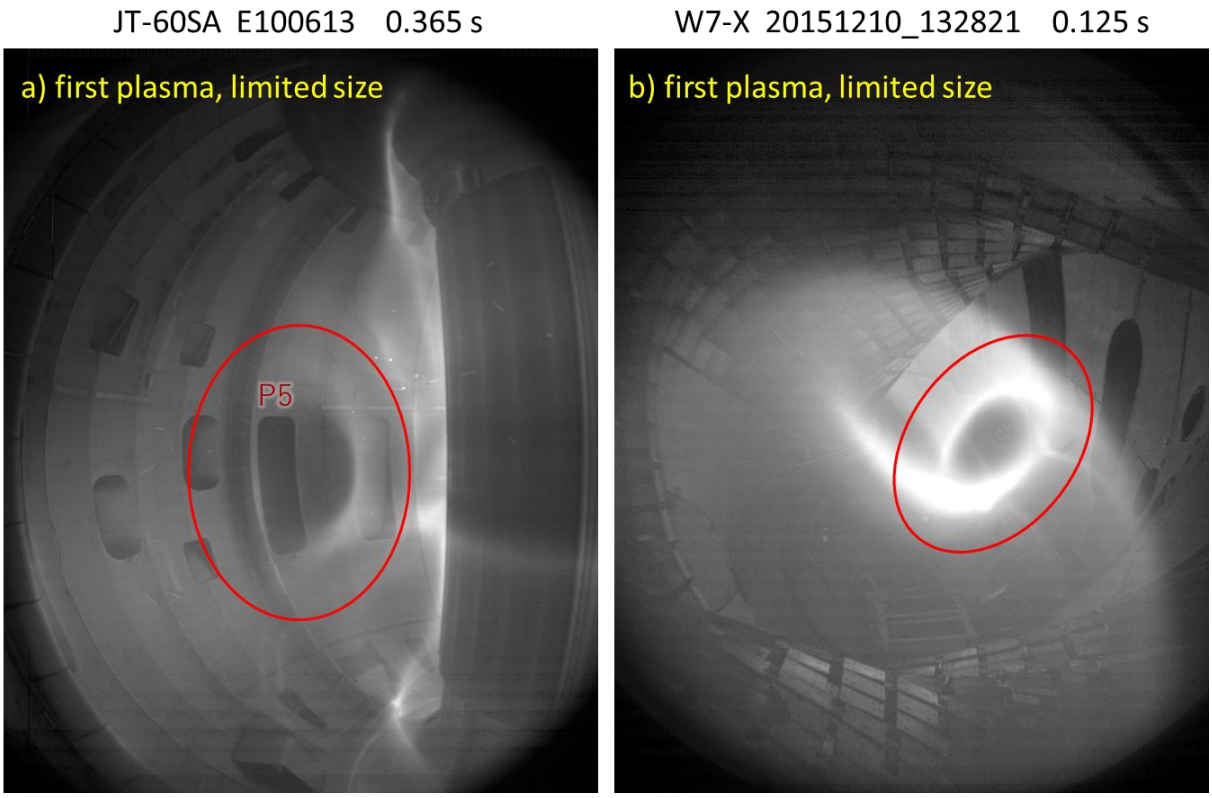

FIG. 2. First successful plasmas at JT-60SA (a) and Wendelstein 7-X (b). The formation of closed flux surfaces and a hot bulk plasma core is shown by the presence of a quasi-circular radiation belt. Yet the plasma remains small compared to the available space in the vacuum vessel.

When the plasma gets in contact with the limiter(s) or divertor(s), in addition to the main plasma species, impurities (mostly carbon or tungsten) from the plasma-facing components enter the plasma, further increasing the intensity of line emissions in localized regions. This translates to visible camera images dominated by strong plasma-wall interactions at these contact locations, as well as reflections from all other in-vessel components, making the radiation belt much less pronounced or even completely invisible. This change in the emission pattern is so obvious that one can tell without any doubt that plasma column has fully formed; this result is an important milestone of a machine's start-up campaign, which can be easily confirmed using a visible video diagnostic system.

3. RUNAWAY ELECTRON DETECTION

The EDICAM system in JT-60SA was designed with a clockwise viewing direction (from above), which matches the direction of both the toroidal magnetic field and the plasma current (see *FIG. 3*.). Hence, in case runaway

electrons (REs) are generated in the tokamak, the EDICAM has the proper view to observe their synchrotron emission as well.

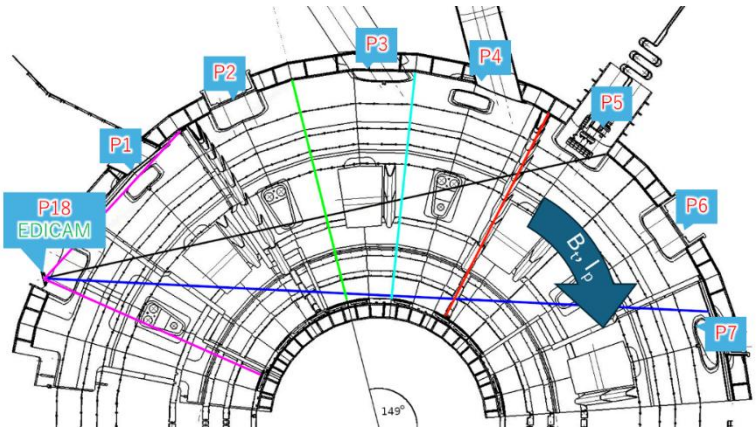

FIG. 3. The geometry of the EDICAM camera view and the direction of the toroidal magnetic field (B_t) and plasma current (I_p) in JT-60SA.

Previous modelling work was carried out for studying the sensitivity of the camera for REs produced in disruptions of the highest-power plasma scenarios. The study reveals that the synchrotron emission is expected to produce a bright crescent-shaped pattern at the inboard of the torus [10], however, it does not provide any information on whether the EDICAM could observe RE activity in the low-power plasmas of IC&OP1. The latter was nevertheless proved experimentally during the first campaign, as the synchrotron radiation of runaway electrons produced during the ramp-down phase of a discharge was clearly observed by the camera. *FIG. 4*. shows two snapshots from the same plasma discharge without (a) and with (b) runaway electron activity. The crescent-shaped emission pattern of the synchrotron radiation in image (b) is distinctive (highlighted by a red rectangle). In this measurement we made use of the fact that EDICAM was not equipped with any interference filter.

Additionally to the crescent-shaped emission pattern, the presence of REs can also be detected indirectly with the camera. The EDICAM has a CMOS sensor, being sensitive for high-energy photons, which in turn can be utilized for hard X-ray (HXR) dosimetry. The effect of high-energy (gamma) photons on the EDICAM's CMOS sensor has been investigated in depth [11], focusing on the radiation damage and the average dark current levels during irradiation. Here, a general numerical method is used for HXR dose rate detection with CMOS sensors. The camera is located about 30 cm away from the confined plasma with no dedicated shielding, just the stainless-steel immersion tube is in the way of the ionizing radiation, which hence can reach the CMOS sensor. In case of high-energy photon - solid-state detector pixel interaction, photoelectrons are generated with significantly higher rate than for visible range photons. This results in a "hot pixel" in the picture, having a significantly higher intensity than the neighbouring pixels, enabling the measurement of the high-energy photon current quantitatively: the hot pixel density in the picture is proportional to the ionizing dose reaching the CMOS sensor, and the hot pixel density normalized with the camera exposure time is proportional to the HXR dose rate in the given environment.

This method can be used for the detection of runaway electron activity with the EDICAM, as the RE beam – wall interaction generates Bremsstrahlung with a hard X-ray component, which can reach the sensor. Hot pixel density is calculated in an "unused" part of the image (upper left or lower left corner), where the imaging shows strong vignetting (see green dashed rectangles in *FIG. 4*.).

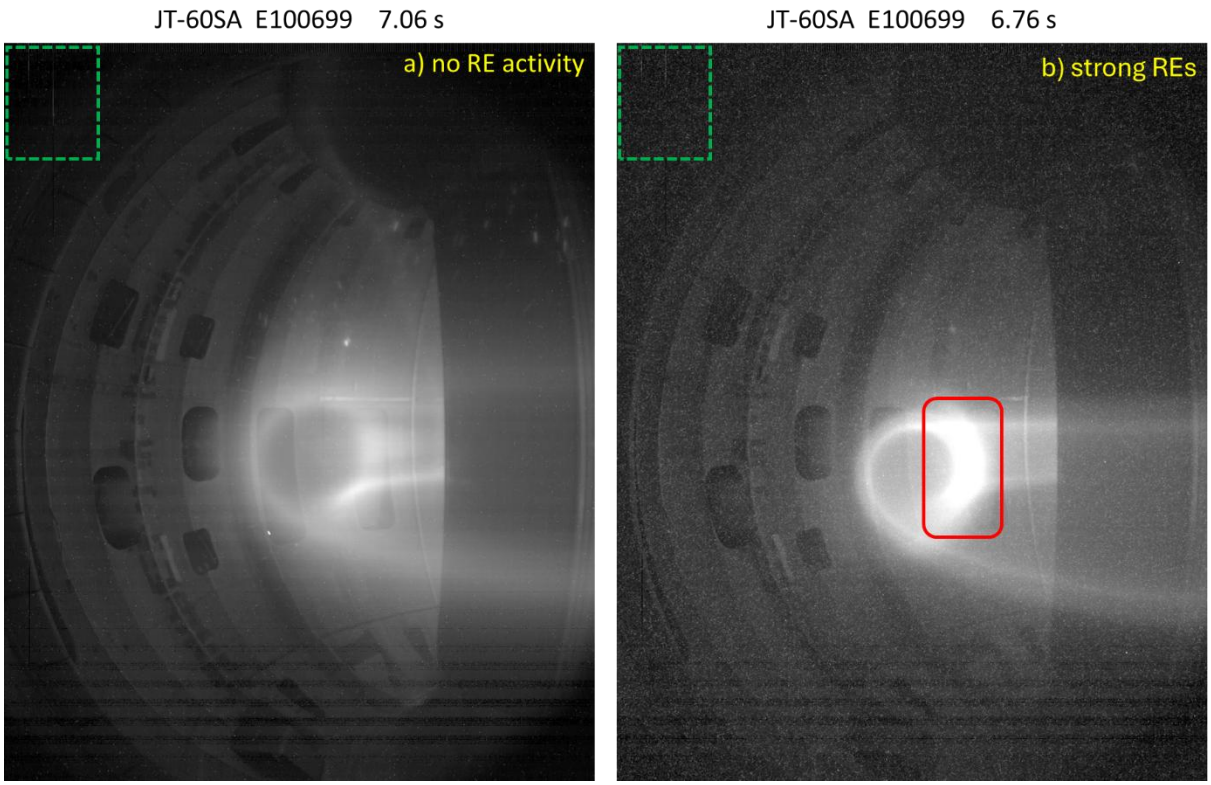

FIG. 4. EDICAM images showing the same plasma discharge in JT-60SA without (a) and with (b) runaway electron activity. The crescent-shaped emission pattern of the synchrotron radiation is highlighted by a red rectangle. Note the increase in image noise level (hot pixels) during RE activity – especially in dark regions (green dashed rectangle).

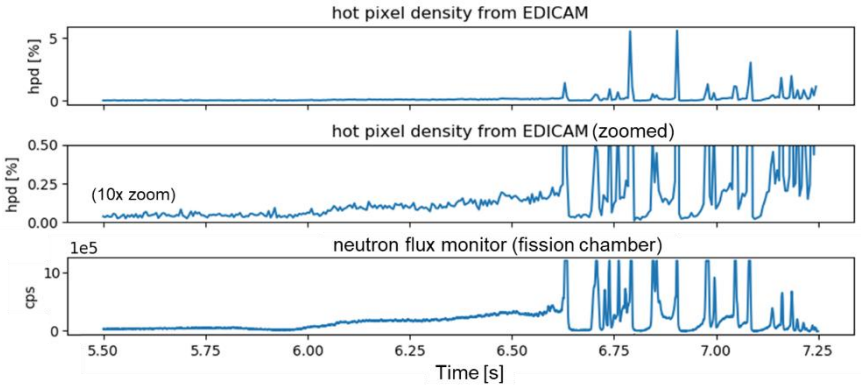

FIG. 5. EDICAM hot pixel density in JT-60SA, discharge E100699 with a RE beam during the ramp-down.

The result of such a hot pixel density analysis can be seen in *FIG. 5*., showing that the hot pixel density is close to zero throughout the discharge (E100699), starts to increase after 6 s during the ramp-down, and shows a very intermittent behaviour during the RE beam activity between 6.6 - 7.3 s, after which the discharge is terminated. Although there was no dedicated HXR diagnostics on JT-60SA during IC&OP1, there are two neutron flux monitors (NFM), one of them also in P18 (just like EDICAM). These are fission chamber type detectors, also sensitive for high energy photons, which offers a possibility for signal comparison with the EDICAM hot pixel density. *FIG. 5*. shows the NFM intensity and the EDICAM hot pixel density time traces (the middle plot is just a vertically zoomed version). The wave form of these signals shows high level of similarity, even during the intermittent phase. There is a clear correlation between the hot pixel density and the NFM signals, showing that the EDICAM can indeed be used as a hard X-ray dosimeter. The comparison reveals that EDICAM and the NFM are comparably sensitive for the ionizing radiation, being linear in the low dose rate ranges, however, the EDICAM has a lower signal-to-noise ratio. On the other hand, the NFM detectors are saturated when the RE beam

activity is high, while the EDICAM hot pixel density reaches only about 5%, i.e. the HXR detection method based on the EDICAM offers a wider dynamic range than the NFM detectors.

4. DETACHMENT DETECTION

Detachment, a plasma state with strongly reduced divertor heat loads, is routinely achieved at W7-X by increasing the radiation level equivalent to 70-90% of the heating power. During detachment, the visible emission of the plasma also increases, resulting in generally brighter images. The visible emission pattern of the plasma also changes: the intensity decreases in the divertor region, the plasma shrinks a little, and a very bright radiation belt emerges.

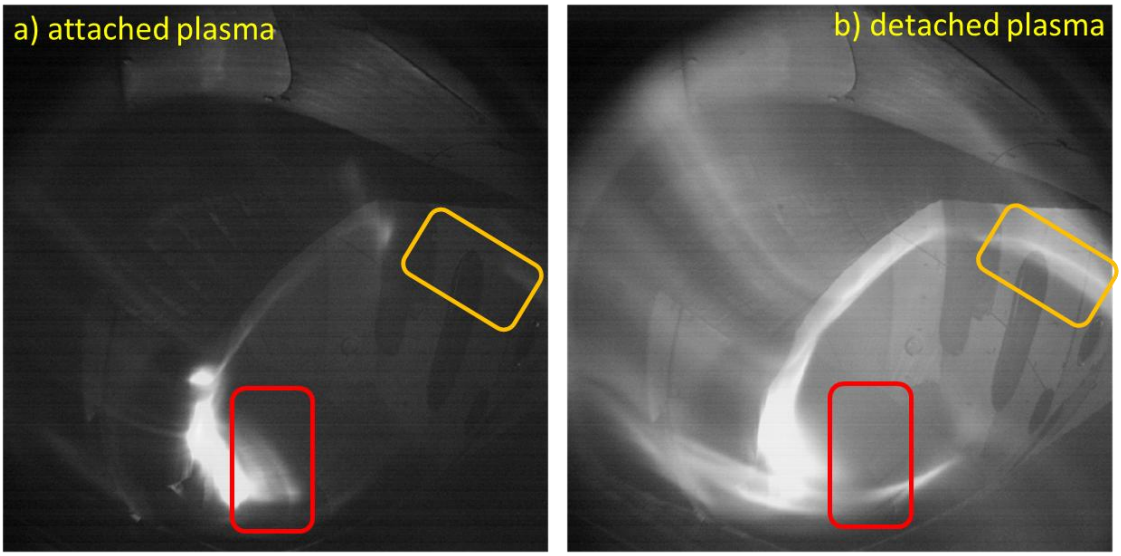

FIG. 6. Differences in the visible radiation pattern of attached (a) and detached (b) plasmas at Wendelstein 7-X.

These changes are characteristic enough for applying simple machine learning (ML) techniques for the automatic detection of detachment. Logistic regression is an efficient and fast ML method, which was applied to W7-X EDICAM data to train on the detection of the detached state. The training dataset was deliberately assembled such that other phenomena, e.g. small plasmas [12] or a change in the magnetic configuration, are successfully ignored. The algorithm delivers very promising results with an F1-score of 0.933 and an area under the ROC curve of 0.972 on the evaluation dataset. An example for the evaluation output is shown in *FIG. 7*.

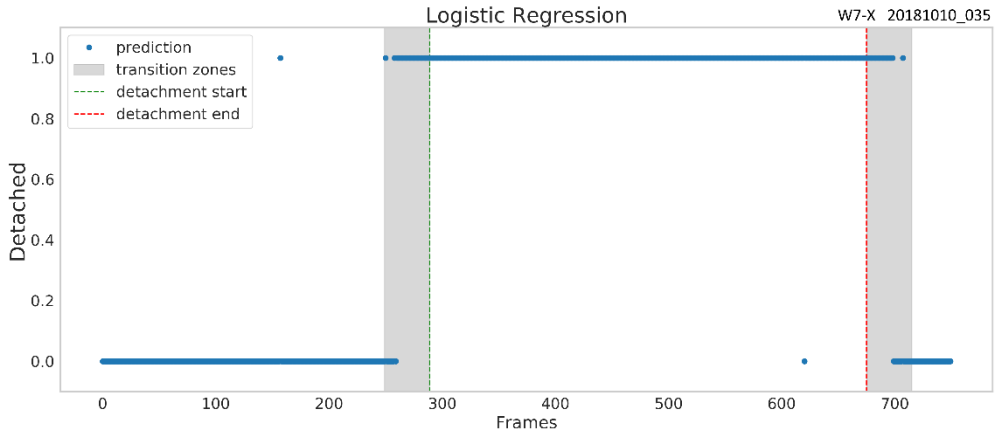

FIG. 7. Results of a trained logistic regression model on the detection of detachment in W7-X EDICAM images. The onset and the end of the detached phase are shown by dashed vertical green and red lines, respectively. The quality of the method is not evaluated in the transition phases (shaded gray areas).

5. CONCLUSIONS

The paper highlights, in addition to the well-established capabilities, the promising potential of standard visible video diagnostics, which may play a crucial role also in the early operational campaigns of future magnetic confinement fusion devices. EDICAM camera recordings from the Wendelstein 7-X stellarator and the JT-60SA tokamak were employed during start-up campaigns to optimize magnetic and heating scenarios, thereby facilitating successful plasma discharges. Operators relied on camera images to assess how the plasma responded to pre-programmed schemes.

During the first operational campaign of JT-60SA, EDICAM recordings provided continuous monitoring of the experiment, from the initial breakdown attempts to the achievement of 1 MA diverted plasmas with a 5-s flat-top. Owing to the foresighted design of the diagnostic, synchrotron radiation from runaway electrons could also be directly observed, alerting operators to this potentially hazardous phenomenon. Furthermore, an image evaluation method based on measuring the density of hot pixels in a predefined image region was developed to provide a quantitative measure of runaway electron activity. This method can also be applied in situations where direct observation of synchrotron radiation is not feasible.

Wendelstein 7-X has now moved well beyond its start-up phase and is currently focused on demonstrating steady-state-capable concepts. Divertor detachment is one such technique, mitigating the extreme heat loads on the divertor. Detachment is achieved through tailoring plasma radiation, which is also prominent in the visible spectrum, thus enabling direct observation using visible cameras. A simple machine-learning approach – logistic regression – was successfully applied at W7-X for the automatic detection of divertor detachment using EDICAM images alone. The simplicity of this method makes it a strong candidate for future implementation in real-time control systems.

ACKNOWLEDGEMENTS

This work has been carried out within the framework of the EUROfusion Consortium, funded by the European Union via the Euratom Research and Training Programme (Grant Agreement No 101052200 — EUROfusion). Views and opinions expressed are however those of the author(s) only and do not necessarily reflect those of the European Union or the European Commission. Neither the European Union nor the European Commission can be held responsible for them.

REFERENCES

[1] YOSHIDA, M. et al, Overview of plasma operation and control studies in the first plasma campaign of JT-60SA, Plasma Phys. Control. Fusion **67** (2025) 065010
[2] WOLF, R. C. et al, Major results from the first plasma campaign of the Wendelstein 7-X stellarator, Nucl. Fusion **57** (2017) 102020
[3] KAMADA, Y. et al, Completion of JT-60SA construction and contribution to ITER, Nucl. Fusion **62** (2022) 042002
[4] KÖNIG, R. et al, The set of diagnostics for the first operation campaign of the Wendelstein 7-X stellarator, J. of Instrumentation **10** (2015) P10002
[5] ZOLETNIK, S. et al, EDICAM (Event Detection Intelligent Camera), Fus. Eng. Des. **88** (2013) 1405
[6] SZEPESI, T. et al, Wide-angle visible video diagnostics for JT-60SA utilizing EDICAM, Fus. Eng. Des. **153** (2020) 111505
[7] KOCSIS, G. et al, Overview video diagnostics for the W7-X stellarator, Fus. Eng. Des. **96–97** (2015) 808–811
[8] SZEPESI, T. et al, Analysis of the first plasmas of JT-60SA using the EDICAM visible video diagnostic, Fus. Eng. Des. (in preparation)
[9] BUZÁS, A. et al, Estimating plasma size by visible emission patterns in the Wendelstein 7-X stellarator, Fus. Eng. Des. **220** (2025) 115304
[10] OLASZ, S. et al, Feasibility of the EDICAM camera for runaway electron detection in JT-60SA disruptions, Fus. Eng. Des. **195** (2023) 113940
[11] NÁFRÁDI, G. et al, Analysis of dark current images of a CMOS camera during gamma irradiation, Fus. Eng. Des. **88** (2013) 3169-3175
[12] PANDEY, A. et al, Stable small plasmas at the density limit in the W7-X stellarator, Phys. Rev. Lett. (in press)